ARCHIVES OF MECHANICS
Arch. Mech. **77** (6), 595–620, 2025, https://doi.org/10.24423/aom.4713

Planar plasma source and a floating wall

A. RIAZANTSEV[1)], Z. PERADZYŃSKI[2)]

[1)] *Institute of Plasma Physics and Laser Microfusion, 23 Hery Street, 01-497 Warsaw, Poland, e-mail: arsenii.riazantsev@ifpilm.pl*

[2)] *Military University of Technology, 2 gen. Sylwestra Kaliskiego Street, 00-908 Warsaw, Poland*

The Debye sheath that forms at the plasma-wall interface is discussed by means of the one dimensional collisionless kinetic model. We pay special attention to the simplification often adopted both in theoretical descriptions and numerical simulations, treating the wall as a perfect absorber. We show that this assumption, although it greatly simplifies the considerations, is too restrictive from the physical point of view as it leads to an overdetermined problem. This becomes somewhat understandable if we notice that this assumption does not allow for taking into account any properties of the wall.

Key words: Debye sheath, collisionless plasma, plasma-wall interactions, collisionless kinetic model.

1. Introduction

The Debye sheath, being an interface between plasma and a floating wall, is characterized by substantial deviations from quasineutrality. The sheath is formed due to disparities between electron and ion masses ($m_e \ll m_i$) and possible temperature differences ($T_e \geq T_i$), such that at the initial stage there exists prevalence of electron over ion incident fluxes towards the wall and the negative charge starts accumulating inside the wall and on its surface. This induces an electric field that accelerates ions and repels electrons to maintain current balance of the charged particles. It is often assumed [1–4] that, at equilibrium, when stationary conditions are achieved, the wall acts as a perfect absorber. The perfect absorber assumption means that the electric field increases (i.e., negative wall charge accumulates) until the charge flux of incident electrons exactly balances the charge flux of ions bombarding the wall. Then, as a result of three-body collisions (ion-electron-wall), the charge flux is neutralized and the particles leave the wall as neutrals. One can imagine that even if some ions bounce off the wall they become trapped by the electric field and retain near the wall until they recombine with electrons that, in the presence

of the repelling electric field, are expected to reach the wall with reduced flux and energy and thus decreasing the probability of electron backscattering to plasma. However, it appears that in case of a perfect absorber, the electric field, and consequently the surface density of absorbed electrons, is uniquely determined by the efficiency of the plasma source and the distance L between the source and the wall. So, it does not depend on the material of the wall or its temperature, which seems unlikely. In other words, assuming an ideal absorber makes the problem overdetermined. For example, by heating the wall, one should be able to reduce the number of electrons absorbed and consequently the wall electric field E_L. If we accept the point of view that we have some control over the absorbing properties of the wall, then a solution representing the electrical structure of the sheath should exist for a specified a priori not only source efficiency and the domain size L but also for the prescribed arbitrarily electric field E_L at the wall surface. The perfect absorber assumption does not offer such a possibility, hence it is very restrictive. It becomes clear that to avoid these limitations one must allow that at equilibrium, when the solution has reached the steady-state, some electrons may still be reflected from the wall and return to plasma. The problem of inadequacy of the perfect absorber assumption is also discussed by Bronold *et al.* [5]. It was noticed that even if the assumption of a perfect absorber was indeed fulfilled in the final state, it cannot describe well the process of reaching this state, causing, for example, inaccuracies in the estimation of the sheath formation time. It seems reasonable to distinct the perfect absorber approximation as a wall property and as a final state. As a wall property it simply implies no emission of electric charge from the surface (including reflection) at any point of time. Whereas the perfect absorber approximation as a final state implies that when the sheath is finally formed the incident fluxes of charged electrons and ions balance each other.

Unlike the work by Bronold *et al.* [5], that focuses on the processes inside and in the vicinity of the wall together with the dynamics of the charge build-up, we intend to show another issue of the perfect absorber approximation, without going into details about the physics of intricate interactions [6, 7] of the plasma particles with the wall. In particular, we aim to emphasize that the plasma-wall problem with stated:

- geometry (size),
- plasma source properties,
- electric field at the wall boundary

becomes overspecified if we additionally assume the wall to be a perfect absorber. Let us consider a thin planar plasma source located at $y \in [-\varepsilon, \varepsilon]$ in the middle between two parallel walls, located at $y = -L$ and $y = L$ (see Fig. 1). Due to

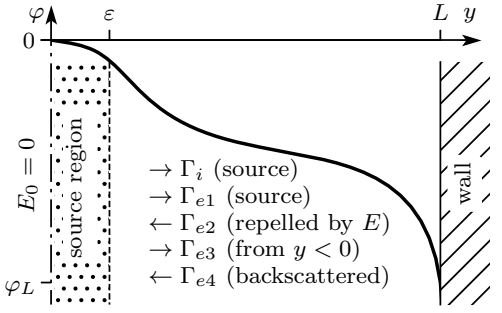

FIG. 1. Problem statement.

evident symmetry we further consider only a half of the problem domain (the one with positive y).

The source produces electrons and ions at the same rate but also transfers additional energy to plasma particles crossing it. Interaction of plasma with the wall, macroscopically, can be characterized by accumulation of certain charge at its surface with the flux balance for the charged particles at the wall [5, 8]:

$$\frac{\mathrm{d}n_e^{(\mathrm{S})}}{\mathrm{d}t} = s_e\Gamma_{e,inc} - \frac{n_e^{(\mathrm{S})}}{\tau_e} - \alpha_{rw}n_i^{(\mathrm{S})}n_e^{(\mathrm{S})}, \tag{1.1a}$$

$$\frac{\mathrm{d}n_i^{(\mathrm{S})}}{\mathrm{d}t} = s_i\Gamma_{i,inc} - \frac{n_i^{(\mathrm{S})}}{\tau_i} - \alpha_{rw}n_i^{(\mathrm{S})}n_e^{(\mathrm{S})}, \tag{1.1b}$$

where $n_e^{(\mathrm{S})}$, $n_i^{(\mathrm{S})}$ are particle surface densities, $\Gamma_{e,inc}$, $\Gamma_{i,inc}$ – incident fluxes, s_e, s_i – sticking coefficients, τ_e, τ_i – desorption times of electrons and ions, correspondingly, and α_{rw} – wall recombination constant. In the above equation and onward we assume singly charged ions. For the steady-state scenario the left-hand side of Eq. (1.1) vanishes. For simplicity, we additionally assume immediate recombination at the wall, i.e., $\alpha_{rw} \to \infty$. As much more mobile electrons ($m_e \ll m_i$) are expected to initially enter the wall at the higher rate, there should be excess of negative charge inside it. This, together with the assumed immediate recombination, implies $n_i^{(\mathrm{S})} = 0$. Thus, subtracting Eq. (1.1a) from Eq. (1.1b) gives the surface number density of electrons at the wall

$$n_e^{(\mathrm{S})} = \tau_e(s_e\Gamma_{e,inc} - s_i\Gamma_{i,inc}). \tag{1.2}$$

Given the surface charge density $\sigma_w = -en_e^{(\mathrm{S})}$ the electric field is $E_L = -\sigma_w/\varepsilon_0$. It can be inferred from Eq. (1.2) that the electric field is determined by properties of the wall that depend on the choice of material. Moreover, E_L can be also controlled by modifying operating conditions, e.g., the wall can be heated

up to induce thermionic emission, as applied in emissive Langmuir probes [9], or even subjected to light to induce photoemission [10]. This means that, in principle, the wall electric field can be chosen "arbitrarily" and therefore it seems that the problem can be indeed characterized by: the domain size L; properties of the plasma source; the electric field at the wall E_L.

The arbitrariness of the boundary electric field means that we can imagine a situation in which the wall remains completely neutral (i.e., $E_L = 0$). In Section 3 we show that this scenario is inconsistent with the assumption of the perfect absorber. To illustrate this, we specify the wall properties in such a way that some fraction of incident electrons, $\eta \equiv 1 - s_e$, is backscattered from the wall. For simplicity, η does not depend on the incident particle's energy. It is evident that the perfectly absorbing wall corresponds to $\eta = 0$. We show that only a trivial solution exists for $\eta = 0$ and $E_L = 0$. In Section 4 we show that the assumption of the perfectly absorbing wall leads to rigidity of the problem and cannot be met in general if L, the source properties and E_L are set arbitrarily. A solution exists only if L is strongly correlated with E_L. The situation changes if we allow for possibility of some electrons to backscatter and return to the plasma ($\eta > 0$). Then, the solution exists for "arbitrary" values of L, source properties and E_L.

One should keep in mind that the energy independent coefficient of elastic backscattering, η, is just a simplification. For example, Monte Carlo simulations of Polytetrafluoroethylene (PTFE, also known as Teflon) surface bombarded with the monoenergetic electron beam [11] show that the coefficient of elastic backscattering rapidly grows from 0 above 0.8 within the incident electrons' energy range from 0 to 8 eV. The coefficient exponentially decreases with a further increase of the energy. In addition, the coefficient depends on the electron angle of incidence [12]. One should also remember about emission of secondary electrons.

For convenience, we further simplify the discussed problem by setting the half-width of the source region to $\varepsilon \to 0$ and assume L to be small enough (or the plasma to be sparse enough) so that collisions can be neglected. This approach allows to describe both electrons and ions fully kinetically and was already used by some authors in theoretical and numerical considerations of the Debye sheath [13–17].

It is worth to point out that by constricting the source region to the singular plane and treating the collisionless plasma using fully kinetic description we, to some degree, circumvent a commonly used approach that describes the plasma-wall transition by means of a two-scale analysis [18] that separates the problem into two distinct regions: a collisional quasineutral plasma presheath (characterized by negligible growth of electric field towards the wall) and the collisionless sheath (characterized by strong deviation from quasineutrality and, therefore, the electric field is much larger compared to the quasineutral region). In the

frame of the two-scale analysis it was shown by BOHM [19] that the existence of the collisionless sheath region requires ions to be pre-accelerated in the presheath to at least ion acoustic speed ($V_i \geq C_s = \sqrt{kT_e/m_i}$). In the approach discussed by us there are no limitations on the ion velocity entering the collisionless region but, as it is shown later, in situations where the source-collector separation L is much larger than the Debye length λ_D and the source ion velocity does not exceed the ion acoustic one $V_{i0} < C_s$ there are two distinct ("source"' and "wall") sheaths and ions within the "source" sheath are accelerated substantially above the ion acoustic velocity, eliminating the need for the presheath (as was pointed out by SCHWAGER and BIRDSALL [13]). Thus, it can be summarized that in our considerations the particles are produced in the (singular) source region but ions are accelerated above ion acoustic velocities in the collisionless region between the source and the wall, whereas in the standard two-scale analysis both the phenomena occur within the collisional quasineutral presheath region. Of course, quantitatively the potential drop of collisional plasma in contact with a floating wall would be different from what we describe in the present paper, but qualitatively the wall sheath should be quite similar as it is formed by the same mechanism. Historically, the approach used in [13] (the one we rely on) is based on a plane-diode model used in the analysis of a single-ended Q-machine by KUHN [20]. One of the operating regimes of the apparatus is characterized by the monotonic potential drop with the two distinct source and collector sheaths.

The paper is organized as follows. In Section 2 we introduce in greater detail the collisionless plasma source-wall model which is used in later considerations. In Section 3 we consider the Gedankenexperiment that describes a quite artificial, from the physical point of view, scenario in which the electric field at the wall is kept zero, so the wall does not absorb electrons. However, it is assumed that recombination takes place. In Section 4 we show that the perfect absorber approximation makes the problem overspecified and the assumption cannot be met in general for stated source-wall separation L and the arbitrarily chosen electric field E_L. It appears that every L is paired to fixed E_L. The possibility to have arbitrary E_L is regained only after allowing for emission of electrons from the wall. Some brief considerations regarding over-determination of the sheath problem in the presence of collisions are discussed in Section 5. Section 6 contains concluding remarks on the results.

2. The model

The statement of the problem can be described as follows:

1. Plane-symmetric domain $y \in [-L, L]$, with the symmetry plane $y = 0$ bounded by walls at $y = -L$ and $y = L$.

2. Monotonic potential drop from the symmetry plane to the wall.
3. A planar plasma source located at the symmetry plane within a narrow region $y \in [-\varepsilon, \varepsilon]$, $\varepsilon \to 0$:
   (a) the source produces equal fluxes of electrons and ions $\Gamma_i = \Gamma_{e1}$,
   (b) distribution function of the produced ions entering the domain is known $\mathrm{f}_i(v) = n_i f_i(v)$, where f_i is the velocity distribution function such that $\int_{-\infty}^{+\infty} f_i(v)\,\mathrm{d}v = 1$,
   (c) velocity distribution function of electrons entering the domain is known $f_e(v)$.
4. The wall properties are specified, with regard to particles' interactions at the wall. In particular, we assume:
   (a) incident ions entering the wall do not leave it and recombine with electrons,
   (b) incident electrons are partially backscattered without energy losses (in fact, reflected). We assume the probability of backscattering to be independent of the electron's energy and being equal to η. If $f_{e,inc}(v)$ is the velocity distribution function of the incident electrons, then the velocity distribution function of backscattered electrons is $f_{e4}(v) = f_{e,inc}(-v)$. The flux of reflected electrons is $\Gamma_{e4} = \eta\Gamma_{e,inc}$.
5. Returned back electrons gain some extra energy while crossing the symmetry plane (source region) $\int_{-\infty}^{+\infty} v^2 f_{e3}(v)\,\mathrm{d}v > \int_{-\infty}^{+\infty} v^2 f_{e2}(v)\,\mathrm{d}v$. Of course, their flux after crossing the symmetry plane is the same $\Gamma_{e3} = \Gamma_{e2}$. For simplicity, we assume the particles to acquire the energy in a way that their velocity distribution function is equal to that of the source electrons $f_{e3} = f_{e1}$.

We are looking for possibility of getting monotonically decreasing potential in the region between the source and the wall. As the region is assumed to be collisionless the motion of particles is characterized by a constant of motion $q\varphi + \frac{mv^2}{2} = \text{const}$. Under the circumstances, all the ions produced at the source reach the wall. Source electrons with energy below $-e\varphi_L$ return back. The same goes for electrons that enter the region from the opposite side of the source plane Γ_{e3}. The combined flux of returned particles Γ_{e2} as well as the previously mentioned electron fluxes (Γ_{e1} and Γ_{e3}) vary along normal to the wall (their total flux, however, remains constant). Electrons with sufficiently large energy reach the wall and, as we have set previously, partially recombine with the incident ions while the excess of incident electrons $\Gamma_{e4} = \Gamma_i - (\Gamma_{e1} + \Gamma_{e3})|_{y=L}$ is backscattered elastically (in 1D case backscattering is equivalent to specular reflection). At the same time, the total flux balance is $\Gamma_{e2}(y) + \Gamma_{e4} = \Gamma_i - (\Gamma_{e1}(y) + \Gamma_{e3}(y))$, where the left-hand side contains particles that move in negative direction, while the right-hand side includes particles that move in positive direction. The total

flux is constant everywhere (steady-state problem). It was previously mentioned that the returned particles gain some energy in the source region, such that their energy spectrum becomes identical to the source particles. This is because the flux of returned particles should be on average accelerated when passing through the source region in order to be able to cross the source-wall potential barrier at the opposite half of the problem. Otherwise, there would be constant accumulation of particles in the region.

For simplicity, we assume the source to produce particles with half-Maxwellian velocity distributions. Taking into account the above considerations the ion distribution function is simply

$$\mathrm{f}_i(\varphi, v) = n_i^* \left(\frac{m_i}{2\pi k T_i}\right)^{1/2} \exp\left(-\frac{m_i v^2}{2kT_i} - \frac{e\varphi}{kT_i}\right) H(v - v_{ic}(\varphi)), \tag{2.1}$$

where $v_{ic} = \sqrt{-2e\varphi/m_i}$ is the ion cut-off velocity. The total electron distribution function is the sum of cut-half-Maxwellians and at arbitrary point $y(\varphi)$ can be written as

$$\begin{aligned} &\mathrm{f}_e(\varphi, v) \\ &\quad = n_e^* \left(\frac{m_e}{2\pi k T_e}\right)^{1/2} \exp\left(\frac{e\varphi}{kT_e} - \frac{m_e v^2}{2kT_e}\right) \left[H(v - v_{ec}(\varphi)) + \eta H(v_{ec}(\varphi) - v)\right], \end{aligned} \tag{2.2}$$

where n_e^* – some constant to be found, measured in units of number density, $v_{ec} = -\sqrt{2e(\varphi - \varphi_L)/m_e}$ – electron cut-off velocity, H – the Heaviside step function, η can be interpreted as the ratio of incident to backscattered electron fluxes. It is clear that the first term in square brackets corresponds to electron components with subscripts $e1$, $e2$, $e3$, while the second to $e4$. Moments of the distribution functions give macroscopic parameters of ions and electrons that can be used with the Poisson equation, parametrized for an electric potential being the argument

$$\begin{cases} E = -\frac{\mathrm{d}\varphi}{\mathrm{d}y}, \\ \frac{\mathrm{d}E}{\mathrm{d}y} = \frac{\rho}{\varepsilon_0}, \end{cases} \quad \rightarrow \quad \begin{cases} \frac{\mathrm{d}y}{\mathrm{d}\varphi} = -\frac{1}{E}, \\ \frac{\mathrm{d}(E^2)}{\mathrm{d}\varphi} = -\frac{2\rho}{\varepsilon_0}. \end{cases} \tag{2.3}$$

By assuming all the variables that correspond to the particle production to be known (in particular, $\Gamma_i(m_i, T_i, n_i^*)$, T_e) it is possible to obtain the electron density constant n_e^* from the flux balance

$$\Gamma_e(n_e^*, \varphi_L, \eta) = \Gamma_i. \tag{2.4}$$

Moreover, using the fact that all the macroscopic variables are defined in terms of electric potential, it becomes possible to integrate Eq. (2.3) to obtain a (closed) system that consists of two equations, namely:

definition of the electric field at the wall

$$E_L^2 = 0 = \frac{2e}{\varepsilon_0}\int_0^{\varphi_L}(n_e(\varphi,\varphi_L,\eta) - n_i(\varphi))\,\mathrm{d}\varphi, \tag{2.5a}$$

definition of the distance between the source and the wall

$$L = -\int_0^{\varphi_L}\left(\frac{2e}{\varepsilon_0}\int_0^{\varphi}(n_e(\acute{\varphi},\varphi_L,\eta) - n_i(\acute{\varphi}))\mathrm{d}\acute{\varphi}\right)^{-1/2}\mathrm{d}\varphi. \tag{2.5b}$$

The explicitly written arguments in system of Eq. (2.5) represent independent variables (φ_L, η) and variables of integration (φ and $\acute{\varphi}$). It is clear that for a specified distance between the source and the wall L and the fact that $E_L = 0$ the system of two equations has two unknowns φ_L, η and is thus closed.

For the sake of convenience we introduce dimensionless variables $\tau = T_e/T_i$, $\mu = m_i/m_e$, $\psi = e\varphi/(kT_e)$. Since the particle production is kept constant and for the Maxwellian source being equal to $\Gamma_i = 0.5n_i^*\langle|v_{iy}|\rangle = 0.5n_i^*\sqrt{2kT_i/(\pi m_i)}$ we additionally introduce $\nu = n/n_i^*$ and $u = v/\langle|v_{iy}|\rangle$, so that the normalized total production (in both directions) is equal to unity with normalized fluxes $\gamma = \Gamma/(2\Gamma_i)$.

Normalized distribution functions become

$$\tilde{\mathrm{f}}_i(\psi,u) = \frac{1}{\pi}\exp\left(-\frac{u^2}{\pi} - \tau\psi\right)H(u-u_{ic}), \tag{2.6}$$

where $u_{ic} = \sqrt{-\pi\tau\psi}$ and

$$\tilde{\mathrm{f}}_e(\psi,u,\psi_L,\eta) = \frac{1}{\pi}\frac{n_e^*}{n_i^*}\frac{1}{\sqrt{\mu\tau}}\exp\left(\psi - \frac{u^2}{\pi\mu\tau}\right)\left[H(u-u_{ec}) + \eta H(u_{ec}-u)\right], \tag{2.7}$$

where $u_{ec} = -\sqrt{\pi\mu\tau(\psi-\psi_L)}$. The ratio of the source ion density and the electrons density constant can be obtained from the flux balance using first moments of the distribution functions $\gamma_i = 0.5$ and $\gamma_e = 0.5(1-\eta)n_e^*/n_i^*\sqrt{\mu\tau}\exp(\psi_L)$, giving

$$\frac{n_e^*}{n_i^*} = \frac{1}{\sqrt{\mu\tau}}\frac{\exp(-\psi_L)}{1-\eta}. \tag{2.8}$$

Zero's moments of the distribution functions give normalized densities:

$$\nu_i(\psi) = \frac{1}{2}\exp(-\tau\psi)\,\mathrm{erfc}\sqrt{-\tau\psi}, \tag{2.9}$$

$$\nu_e(\psi,\psi_L,\eta) = \frac{1}{2\sqrt{\mu\tau}}\exp(\psi-\psi_L)\left[\frac{2}{1-\eta} - \mathrm{erfc}\sqrt{\psi-\psi_L}\right]. \tag{2.10}$$

System of Eqs. (2.5) is rewritten by introducing dimensionless variables $\upsilon = y/\lambda_D^*$ and $\xi = E\frac{\lambda_D^* e}{kT_e}$, where $\lambda_D^* = \sqrt{\varepsilon_0 kT_e/(n_i^* e^2)}$ – is the Debye length of the source plasma, yielding:

$$\xi_L^2(\psi_L,\eta) = -2\int_0^{\psi_L}(\nu_i(\psi) - \nu_e(\psi,\psi_L,\eta))\,\mathrm{d}\psi, \tag{2.11a}$$

$$\upsilon_L(\psi_L,\eta) = -\int_0^{\psi_L}\frac{\mathrm{d}\acute{\psi}}{\sqrt{\xi^2(\acute{\psi},\psi_L,\eta)}}, \tag{2.11b}$$

where ξ^2 in Eq. (2.11b) is the normalized electric field (squared) at the arbitrary point, which is equivalent to Eq. (2.11a) with the upper limit of density integrals being the normalized potential ψ:

$$\int_0^{\psi}\nu_i(\psi)\,\mathrm{d}\psi = -\frac{1}{2\tau}\left(\exp(-\tau\psi)\operatorname{erfc}\sqrt{-\tau\psi} + \sqrt{-\frac{4\tau\psi}{\pi}} - 1\right), \tag{2.12}$$

$$\begin{aligned}\int_0^{\psi}\nu_e(\psi,\psi_L,\eta)\,\mathrm{d}\psi = \frac{1}{2\sqrt{\mu\tau}}\Bigg[&\exp(\psi-\psi_L)\left(\frac{2}{1-\eta} - \operatorname{erfc}\sqrt{\psi-\psi_L}\right)\\ &- \exp(-\psi_L)\left(\frac{2}{1-\eta} - \operatorname{erfc}\sqrt{-\psi_L}\right) - \sqrt{\frac{4}{\pi}(\psi-\psi_L)} + \sqrt{-\frac{4}{\pi}\psi_L}\Bigg],\end{aligned} \tag{2.13}$$

and the normalized ion-density integral in Eq. (2.11a) is obviously equal to Eq. (2.12) with the upper limit being ψ_L, while the normalized electron density integral can be simplified to

$$\begin{aligned}\int_0^{\psi_L}\nu_e(\psi,\psi_L,\eta)\,\mathrm{d}\psi = \frac{1}{2\sqrt{\mu\tau}}\Bigg[&\frac{2}{1-\eta}(1-\exp(-\psi_L))\\ &+ \exp(-\psi_L)\operatorname{erfc}\sqrt{-\psi_L} + \sqrt{-\frac{4}{\pi}\psi_L} - 1\Bigg].\end{aligned} \tag{2.14}$$

Given the mass ratio of the particles μ and the ratio of the source temperatures τ system of Eqs. (2.11) becomes closed for the specified "length" υ_L and wall charge ("electric field" ξ_L). For convenience, the dimensionless variables are summarized in Table 1.

TABLE 1. Relations between dimensional and dimensionless variables.

Dimensionless variable	Definition
Ion-to-electron mass ratio	$\mu = m_i/m_e$
Ion-to-electron temperature ratio	$\tau = T_e/T_i$
Density of species α	$\nu_\alpha = n_\alpha/n_i^*$
Flux of species α	$\gamma_\alpha = \Gamma_\alpha/(2\Gamma_i) = \Gamma_\alpha/(n_i^*\langle\|v_{iy}\|\rangle)$
Velocity of species α	$u_\alpha = v_\alpha/\langle\|v_{iy}\|\rangle$
Spatial y-coordinate	$\upsilon = y/\lambda_D^*$
Electric potential	$\psi = e\varphi/(kT_e)$
Electric field	$\xi = eE\lambda_D^*/(kT_e)$

3. Uncharged wall scenario

As mentioned before, expecting the wall charge to be capable of taking "arbitrary" values, we start from an extreme artificial case of the completely uncharged wall. Then, the adequacy of the zero wall charge scenario against the previously introduced weak perfect absorber approximation can be tested in the frame of the discussed model. Let us recall that the weak perfect absorber approximation means that the potential drop between the source and the wall is so large that all electrons reaching the wall recombine with ions located there. In a general case, assuming mass and temperature disparities of electrons and ions, the scenario for which the wall remains neutral is expected when the excess of incident electrons (not participating in recombination) is compensated by an electron flux from the wall. This excess, represented in the model by the coefficient η, can be obtained for the case of the uncharged wall $\xi_L = 0$ by rewriting Eq. (2.11a) of the system as

$$\eta(\psi_L) = 1 + \frac{2(1-\exp(-\psi_L))}{\sqrt{\frac{\mu}{\tau}}\left(\exp(-\tau\psi_L)\operatorname{erfc}\sqrt{-\tau\psi_L} + \sqrt{-\frac{4\tau\psi_L}{\pi}} - 1\right) + \exp(\psi_L)\operatorname{erfc}\sqrt{-\psi_L} + \sqrt{-\frac{4\psi_L}{\pi}} - 1}. \tag{3.1}$$

The parametric space of system of Eqs. (2.11) is visualized in Fig. 2. From now on and for the entire paper we provide calculations for atomic hydrogen $\mu = m_{i,H}/m_e \approx 1837$ and $\tau = 100$. Not every solution appears to be physical. One can notice that possible values of the normalized wall potential ψ_L lie within a range from 0 to some negative value and further decrease of ψ_L would result in the complex-valued normalized electric field ($\xi^2 < 0$, see middle plot), which is unphysical. The right-most plot in Fig. 2 shows that every physical wall potential ψ_L corresponds to unique distance υ_L.

The results indicate that for given source properties it is not possible to obtain a solution with zero electric field at the wall and equal number of electrons

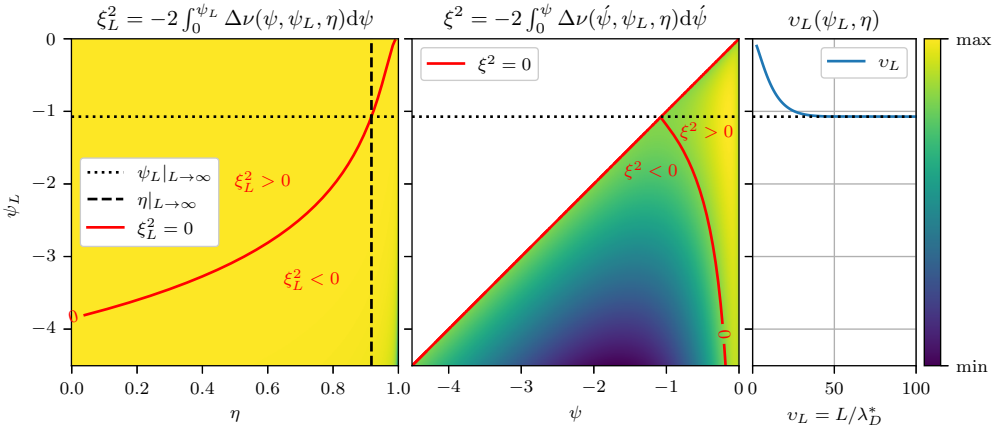

FIG. 2. Solution space of system of Eqs. (2.11). The left colormap depicts normalized electric field at the wall ξ_L^2 with the red isoline showing a relation between normalized wall potential ψ_L and ratio of incident to backscattered electrons η for which the electric field at the wall vanishes $\xi_L = 0$. We denote for brevity $\Delta\nu = \nu_i - \nu_e$. The middle colormap shows distribution of normalized electric field ξ^2 between the source and the wall for different ψ_L and η. The red isoline corresponds to zero local electric field $\xi^2 = 0$. The right plot shows the relation between ψ_L and the normalized source-wall separation υ_L. The black dotted line in all three plots indicates the smallest physically possible value of the wall potential (the largest possible potential drop), for which $\upsilon_L \to \infty$.

and ions reaching the wall (the solution for $\eta = 0$ is unphysical). Of course, it would be possible to get some trivial solutions for the above wall conditions, for example, if ions produced by the source have the same mass and temperature as electrons. However, in this case the potential drop would be zero and the sheath would not appear at all.

4. Charged wall scenario

It has been shown that the assumption about equal fluxes of incident electrons and ions at the wall does not account for arbitrary values of the electric field ξ_L. The rigidity of the problem, brought by this assumption, can be investigated within the frame of the discussed model. The system of Eqs. (2.11) remains unchanged, however, now we exclude the solutions with unequal incident fluxes of electrons and ions by setting $\eta = 0$ but allow for arbitrary values of electric fields at the wall, i.e., ξ_L^2 in Eq. (2.11a) may now take nonzero values. In other words, we fix the backscattering coefficient to reduce solutions of Eq. (2.11a) to a curve in (ψ_L, ξ_L) space. Visualization of the parametric space in Fig. 3 shows that among all possible combinations of ψ_L and ξ_L not all of them are physical. Again, for some of them, the electric field in the region between the source and

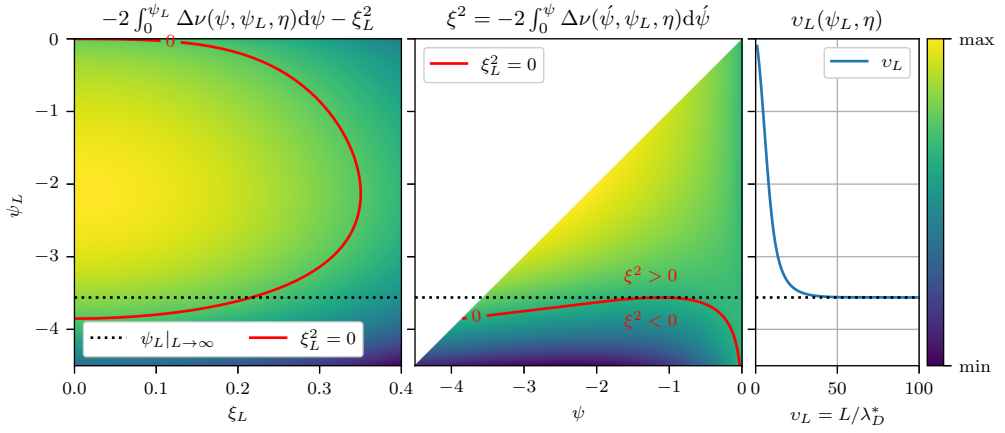

Fig. 3. Solution space of Eq. (2.11) for $\eta = 0$ and arbitrary ξ_L in Eq. (2.11a). The left colormap gives the solutions of Eq. (2.11a), shown as a red isoline, for selected electric field (horizontal axis) and potential (vertical axis) at the wall. The middle colormap shows distribution of normalized electric field ξ^2 between the source and the wall for different ψ_L and η. The red isoline corresponds to zero local electric field $\xi^2 = 0$. The right plot shows unique normalized source-wall separations υ_L that correspond to given solutions. The black dotted line in all three plots indicates the smallest physically possible value of the wall potential (the largest possible potential drop), for which $\upsilon_L \to \infty$.

the wall becomes complex-valued ($\xi^2 < 0$, see middle plot). There are also two zero-field solutions (left plot): one is non-physical, while another is trivial as it corresponds to zero source-wall separation $\upsilon_L = 0$. By looking at the right-most plot one can notice that the smallest physical wall potential (the largest physical potential drop) corresponds to infinite separation $\upsilon_L \to \infty$. In addition, every source-wall separation is uniquely paired to a certain wall potential which, in its turn, is paired (non-uniquely) to a certain electric field. This correlation between the source-wall separation and the wall potential leaves no room for arbitrariness of the electric field at the wall, thus, the problem is overspecified.

4.1. Structure of the monotonic potential drop

It is clearly visible that the infinite length solution in Fig. 3 is tangent to the zero electric field isoline implying $\psi_L|_{\upsilon_L\to\infty}$ to be the only solution with $\xi = 0$ at some point between the source and the wall. This point must be the plateau described in the work by Schwager and Birdsall [13] and was used as an assumption to close the system of equation avoiding the need to specify the electric field at the wall. In the original model [13] the simulation region is characterized by two distinct potential drops: the source sheath and the collector sheath. The source sheath forms to neutralize the particles emitted from the source boundary. Ions in the model reach the Bohm minimum velocity ($V_B \geq C_s = \sqrt{kT_e/mi}$)

before crossing the source sheath. The Bohm criterion ensures that the electric field within the sheath (where plasma is no more treated as collisional) is real-valued. The condition is obtained from analysis of the Poisson equation, assuming cold ions and Boltzmann electrons. The Poisson equation is then transformed into the relation for the squared electric field in the sheath and linearized, giving the criterion of minimum kinetic energy of incident ions at the sheath edge [19] (assuming the electric field there is negligibly small compared to the rest of the sheath). SCHWAGER and BIRDSALL [13] mention that the presence of the source sheath "is obviating the need for a presheath acceleration".

Since we do not make an assumption about the presence of quasineutral region but rather define the electric field at the wall we do not restrict ourselves to Schwager's solution and the problem statement is a priori unaware of quasineutral region and two distinct separate sheaths. If the separate regions exist there should be inflection points of the electric potential profiles $\mathrm{d}E/\mathrm{d}y = \varepsilon_0^{-1}\rho = 0$ or $\mathrm{d}\xi/\mathrm{d}\upsilon = \nu_i - \nu_e = \Delta\nu$ in dimensionless variables. The normalized electric field gradient is depicted in the left plot in Fig. 4. It can be seen that for solutions with ψ_L being below a certain value there exist two inflection points that correspond to borders between three separate regions with concave, convex and then again concave potential profiles. For other solutions the potential profile is always concave (which is natural as the electric field at

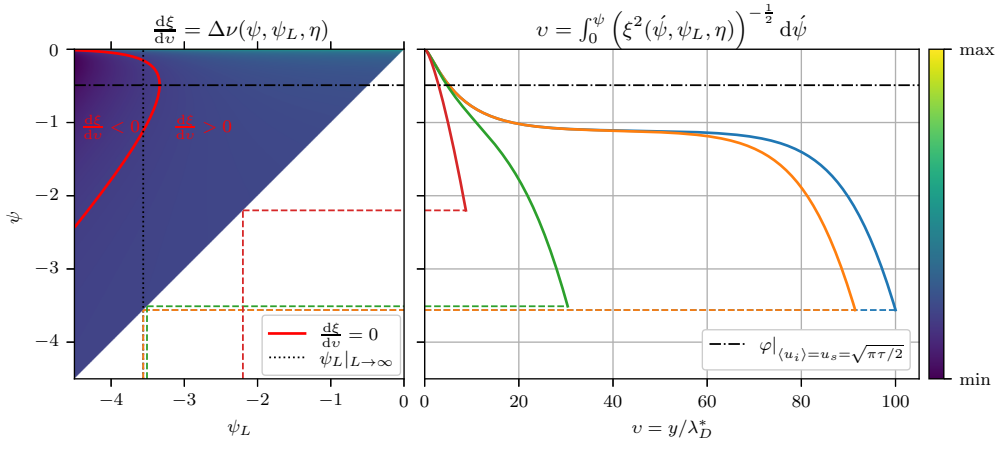

FIG. 4. Gradient of normalized electric field of all possible solutions (left) and corresponding potential profiles as a function of spatial coordinate (right) for the charged wall with $\eta = 0$. The red isoline on the left plot indicates zero gradient of the electric field (zero charge density). The dotted line indicates the smallest physically possible value of the wall potential (the largest possible potential drop), for which $\upsilon_L \to \infty$. The black dash-dotted horizontal line corresponds to ψ for which average ion velocity reaches the value of ion-acoustic speed. As previously, the black dotted line indicates the smallest physically possible value of the wall potential (the largest possible potential drop), for which $\upsilon_L \to \infty$. The dashed lines on both plots indicate the wall potentials ψ_L of the corresponding profiles plotted on the right plot.

the source is set to be zero and the monotonic potential drop is assumed). The right plot in Fig. 4 shows some exemplary spatial distributions of normalized electric potential. Starting from some sufficiently large source-wall separation it becomes clearly seen that the further increase of L only expands the quasi-neutral plasma region (or plateau) while the source and the wall sheaths remain unchanged. It is also worth to point out that normalized plasma density in the quasineutral region is $\nu_i = n_i/n_i^* = 2.66 \cdot 10^{-2}$, which means that it is almost 38 times smaller than plasma density at the source and this would contribute to increase of the local Debye length compared to the source value λ_D^* (roughly by 6 times), however, one must also keep in mind that a decrease in the local electron temperature should contribute to a decrease in the local λ_D.

The wall sheath of the source-wall model should be of the same nature as in the quasineutral plasma sheath model, therefore, to check if Bohm's criterion for ion velocity is satisfied we look at which point ions reach the ion acoustic velocity C_s, which takes the dimensionless form $u_s = \sqrt{\pi\tau/2}$. From constant ion flux and density described by Eq. (2.10) one can inherit that the ion velocity depends only on the local value of the electric potential

$$\langle u_i \rangle(\psi) = \frac{\gamma_i}{\nu_i(\psi)} = \frac{\exp(\tau\psi)}{\operatorname{erfc}\sqrt{-\tau\psi}}. \tag{4.1}$$

The numerically obtained electric potential at which the ion acoustic velocity is reached indicates in Fig. 4. For double sheath solutions the velocity of ions exceeds C_s already at the source sheath, as in [13]. The existence of non-zero electric field for all physical solutions of the finite source-wall separation in the model implies the monotonic potential drop to exist even for velocities below Bohm's limit, however, this sheath is the source sheath not the wall sheath. Such a conclusion arises from the fact that if we consider the second inflection point (the closest to the wall) as the end of the source sheath and beginning of the wall sheath, then the absence of inflection points at all (see the left plot in Fig. 4) means that only the source sheath exists.

To show that ion acoustic velocity is the lowest limit required for the wall sheath to appear we modify the description of ions by assuming them to be monoenergetic with non-zero velocity at the edge of the source region. The ion density for the collisionless case can be obtained from the continuity equation and energy conservation. Keeping the ion production rate the same as in the case of the Maxwellian source the normalized ion density can be represented in the dimensionless units as

$$\nu_i(\psi) = \frac{1}{2\sqrt{u_{i0}^2 - \pi\tau\psi}}. \tag{4.2}$$

The results of using the new relationship for the ion density in a system of Eqs. (2.11) are shown in Fig. 5. The red isoline representing zero of the nor-

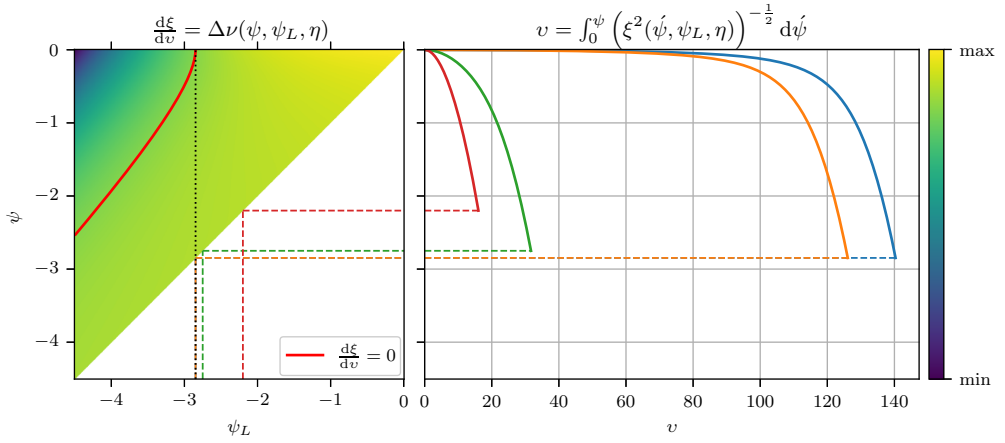

FIG. 5. Gradient of normalized electric field of all possible solutions (left) and corresponding potential profiles as a function of spatial coordinate (right) for the charged wall with $\eta = 0$ and monoenergetic ions that enter the region with ion acoustic velocity $u_s = \sqrt{\pi\tau/2}$. The red isoline on the left plot indicates zero gradient of the electric field (zero charge density). The black dotted line indicates the smallest physically possible value of the wall potential (the largest possible potential drop), for which $v_L \to \infty$. The dashed lines on both plots indicate the wall potentials ψ_L of the corresponding profiles plotted on the right plot.

malized electric field gradient (equivalent of charge density) in the left plot is tangential to the infinite length solution and does not enter the region of other physical solutions. This means that electric potential profiles of these solutions do not have inflection points, which is confirmed by the right plot depicting some selected electric potential profiles.

There are several aspects that make the latter solution different comparing to the traditional calculation of the collisionless sheath region of the two-scale approach. First, while both solutions assume a zero electric field at the sheath entrance, in the two-scale analysis $E_0 = 0$ should be interpreted as the field is negligibly small with respect to the rest of the sheath but appears to be large with respect to the presheath region, while in the discussed approach the field is zero due to symmetry. Second, in the two-scale approach the quasineutrality of plasma at the sheath entrance is actually defined as the strict neutrality $n_i = n_e$, while in the discussed approach the relation between the electron and ion densities depends on L such that for small values $n_e < n_i$ but the difference becomes smaller as $L \to \infty$. Third, electrons in the two-scale approach are assumed to follow the Boltzmann relation $n_e \propto \exp\left(-\frac{e\varphi}{kT_e}\right)$, implying the equilibrium (the Maxwellian velocity distribution), while in the discussed approach the collisionless electrons end up having cut-Maxwellian velocity distribution due to the potential drop, which is closer to the real life situation. However, the effect of assuming Boltzmann electrons appears to be negligible. The potential drop from the two scale analysis can be obtained by equating electron

$\Gamma_e = 0.5 n_{e0} \exp\left(e(\varphi_L - \varphi_0)/(kT_e)\right)\sqrt{2kT_e/(\pi m_e)}$ and ion $\Gamma_i = n_{i0}\sqrt{kT_e/m_i}$ fluxes at the wall. Since the presheath is assumed to be quasineutral $n_{e0} \approx n_{i0}$ and setting $\varphi_0 = 0$, the potential drop is equal to $\varphi_L = 0.5(kT_e/e)\ln(2\pi m_e/m_i)$ or $\psi_L = 0.5\ln(2\pi/\mu)$. For ions of monoatomic hydrogen the calculated value is $\psi_L = -2.84$, while the numerical result of our calculations for the case of infinite source-wall separation, cut-Maxwellian electrons and cold ions with ion acoustic velocity at position $\upsilon = 0$ is $\psi_L = -2.85$. One should keep in mind that the choice of both $V_{i0} = C_s$ and the boundary condition $E_0 = 0$ for the sheath edge in the two-scale analysis is mere an approximation since the electric field at the sheath edge is negligible compared to the rest of the sheath. In fact, there are infinitely many combinations of V_0 and E_0 that give the monotonic potential drop [21], even those allowing for $V_0 < C_s$ but requiring $E_0 > 0$.

4.2. Effects of electron reflection

The rigidity of the problem statement with the assumption of equal incident electron and ion fluxes, mentioned at the beginning of this section, can be inferred from Fig. 3 by the fact that every possible wall potential ψ_L is strongly correlated with the source-wall separation υ_L such that they form unique pairs. Hence, to allow for possibility to impose a different electric field at the wall, the wall properties must be somehow modified. In the frame of the presented model we illustrate this by changing the coefficient of elastic backscattering η. Indeed, as shown in Fig. 6, there is given a fixed distance between the source and the

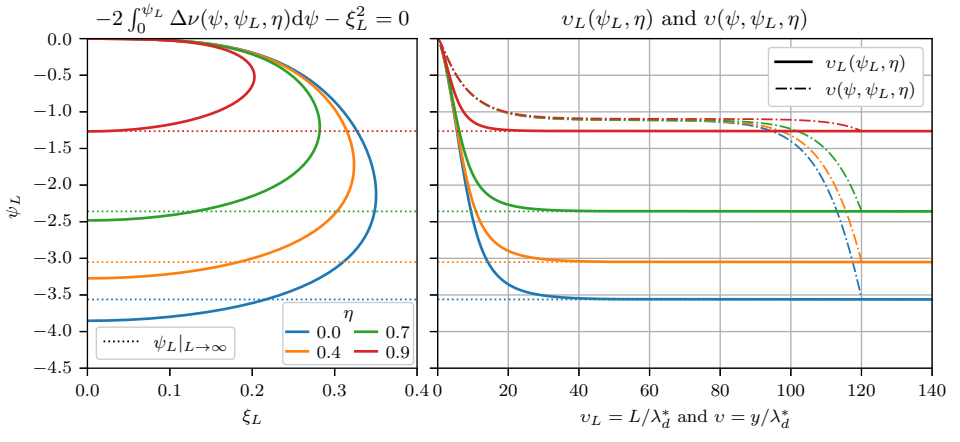

FIG. 6. Solutions of Eq. (2.11) for different η and arbitrary electric field at the wall in Eq. (2.11a). The left plot gives the solutions of Eq. (2.11a) for selected electric field (horizontal axis) and potential (vertical axis) at the wall. The dotted lines indicate the smallest physically possible value of the wall potential (the largest possible potential drop), for which $\upsilon_L \to \infty$. The right plot shows unique lengths that correspond to the given solutions as well as exemplary electric normalized potential profiles for a given η and $\upsilon_L = L/\lambda_D^* = 120$.

wall υ_L, it is now possible to have an "arbitrary" wall electric field, which is bounded in the region between zero and the value that corresponds to the case of the fully absorbing wall ($\eta = 0$) so that $\xi_L \in [0, \xi_L|_{\eta=0}]$. For large fixed source-wall separation the structure of the source sheath remains practically insensitive to electron backscattering from the wall. At the same time the potential drop between the wall sheath decreases with the increase of η. The same goes for an electric field. The situation with $\xi_L = 0$ is exactly the same as that discussed in Section 3 and corresponds to critical ratio of elastic backscattering η_{cr}. This means that all physical results of the uncharged wall problem ($E_L = 0$) in Fig. 2 give critical backscattering coefficients for different source-wall separations. The smallest η_{cr} corresponds to $\upsilon_L \to \infty$ (or $L \to \infty$), as shown by the red isoline on the leftmost plot in Fig. 2. The critical elastic backscattering coefficient η_{cr} constitutes the limit of applicability of the discussed model as increasing η above the critical value would result in reversal of the wall electric field and emergence of a virtual cathode, which contradicts the assumption of monotonic potential drop. The virtual cathode manifests itself as a potential minimum that emerges in the vicinity of the wall. The reversed electric field in the region between the virtual cathode and the wall reduces the emitted electron flux and this scenario is usually called space charge limited emission [9]. The effect of decreasing the potential drop with the increase of emission, for $\eta < \eta_{cr}$, is qualitatively similar to what is shown by HOBBS and WESSON [22] who consider emission of cold electrons from the surface of the wall. The effect allows the plasma potential to be measured using emissive Langmuir probes and the floating potential method [9, 23]. The difference between the plasma potential and the floating potential of the probe (equivalent to $\Delta\psi = \psi_0 - \psi_L$ in the presented model) decreases with the increase of emission until the emitted current becomes space charge

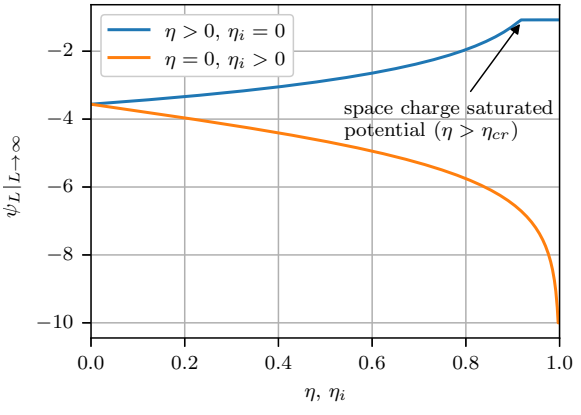

FIG. 7. Electric potential at the wall, ψ_L, as a function of electron, η, and ion, η_i, elastic backscattering coefficients for $L \to \infty$.

limited ($\eta > \eta_{cr}$, equivalently, see Fig. 7), resulting in space charge saturation of the floating potential. The potential difference becomes $\Delta\psi \approx 1$, hence, the measurement error is proportional to plasma electron temperature $\Delta\varphi \approx kT_e/e$.

4.3. Ion reflection

In the above considerations ions were assumed to immediately recombine at the surface of the wall, which is highly probable as, usually, ionization energy is greater than the work function of the wall material. Regarding experimental data on reflection of ions, the experiments are usually made for particles with energies of the order starting from 0.1 to 10 keV [24–26], whereas the energy of ions from quasineutral plasma bombarding the wall is of the order of electron thermal energy. Another issue is that very often by elastic reflection of ions authors mean the ratio of incident ion flux to the reflected flux of recombined neutrals [27–29]. The reflection coefficient as the ratio of incident ions to reflected ions bombarding the tungsten surface is considered by Hagstrum [30], however, the energy range of incident ions is also very large. The reflection coefficients found in that work are negligibly small, ranging from 0.0004 to 0.002. We could not found any other works, describing ion reflection coefficients for other materials and low energy ranges. Nevertheless, we find it necessary to elaborate this question for the sake of completeness. As was shown for the case of electron backscattering, the intensified reflection reduces the potential drop, thus, intuitively, the ion reflection is expected to make ψ_L smaller (increase the potential drop).

Let us consider a scenario when some fraction of incident ions η_i is backscattered (reflected) from the wall. For simplicity, we assume that the reflected particles keep their incident energy and their velocity simply reverses its sign ($\tilde{f}_{i4}(u) = \tilde{f}_{i,inc}(-u))|_{v=v_L}$. In the presence of a monotonic potential drop between the source and the wall, all reflected ions will reach the source such that their velocity distribution function will be identical to that of the source (with the sign reversed) and after crossing the source boundary they will not be distinguished from the source ions even without the refluxing mechanism used for electrons. This means that, within the entire collisionless region $v = (0, v_L)$, the velocity distribution function of reflected ions is the same as the velocity distribution function of the source, with the sign reversed, $(\tilde{f}_{i4}(u) = \tilde{f}_{i1}(-u))|_{v\in(0,v_L)}$ and the "refluxed" ions have exactly the same velocity distribution function as the source ions $(\tilde{f}_{i3}(u) = \tilde{f}_{i1}(u))|_{v\in(0,v_L)}$. We know from the conditions at the wall that (keep in mind that the index number is the same as for electrons)

$$\gamma_{i4} = -\eta_i(\gamma_{i1} + \gamma_{i3}), \tag{4.3}$$

and from the conditions at the source that

$$\gamma_{i4} = -\gamma_{i3}. \tag{4.4}$$

The two flux balances hold true in the entire region $\upsilon = (0, \upsilon_L)$, moreover, each separate flux is kept constant too. From the equality of VDFs we know that the absolute values of average velocities are the same (for certain position $y(\varphi)$) and we can drop them out from the flux balance and determine how the reflected and "refluxed" ion densities relate to the source ion density

$$\gamma_{i3} = \frac{\eta_i}{1-\eta_i}\gamma_{i1} \to \nu_{i3} = \frac{\eta_i}{1-\eta_i} n_{i1} = \nu_{i4}. \tag{4.5}$$

Thus, the total ion density becomes

$$\nu_i = \nu_{i1} + 2\frac{\eta_i}{1-\eta_i}\nu_{i1} = \frac{1+\eta_i}{1-\eta_i}\nu_{i1}. \tag{4.6}$$

The results for different η_i are depicted in Fig. 8. As expected, the potential drop increases with the proportion of reflected ions. The dependency of $\psi_L|_{L\to\infty}$ on η_i is additionally shown in Fig. 7. The width of the source and wall sheaths, shown in Fig. 8, decreases due to an increase of the plasma density and consequent decrease of the local Debye length.

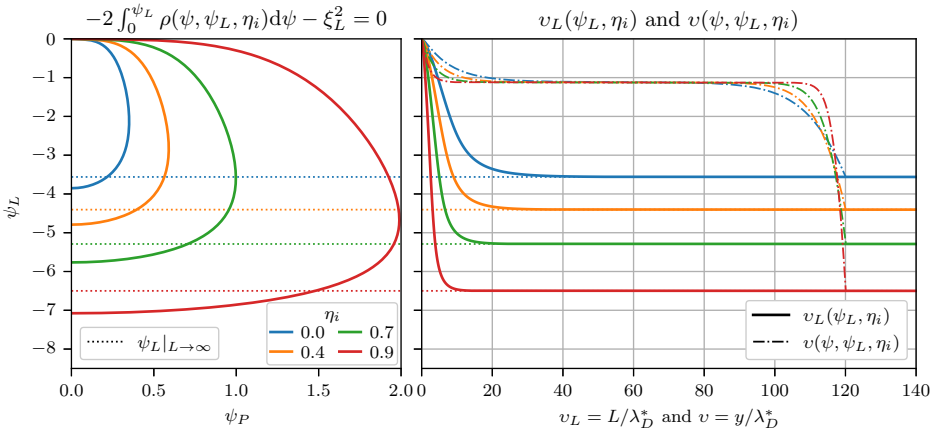

FIG. 8. Solutions of Eq. (2.11) for different η_i and arbitrary electric field at the wall. The left plot gives the solutions of Eq. (2.11a) for selected electric field (horizontal axis) and potential (vertical axis) at the wall. The dotted lines indicate the smallest physically possible value of the wall potential (the largest possible potential drop), for which $\upsilon_L \to \infty$. The right plot shows unique lengths that correspond to the given solutions as well as exemplary electric potential profiles for a given η_i and $\upsilon_L = 120$.

5. Influence of collisions

The question arises whether the presence of collisions can change the results of the considerations regarding the overdetermination of the problem in the case of a perfect absorber. To answer this question, for simplicity, let us consider the

stationary Boltzmann equations for electrons and ions in the BGK (Bhatnagar–Gross–Krook) approximation. As before, we assume that the plasma is homogeneous along planes parallel to the wall, so its parameters depend only on the variable y. For simplicity, we ignore collisions between electrons, assuming that electrons can collide with neutral particles only. In this case, the electron energy remains essentially constant during collisions, and the collisions result in isotropization of the distribution function. Consequently, the electron distribution function satisfies

$$v\frac{\partial}{\partial y}\mathrm{f}_e - \frac{eE}{m_e}\frac{\partial}{\partial v}\mathrm{f}_e = \nu_{ea}(\mathrm{f}_{e,iso} - \mathrm{f}_e), \tag{5.1}$$

where by v we mean the y-component of velocity, $\mathrm{f}_{e,iso}(y,\mathbf{v})$ is obtained by averaging $\mathrm{f}_e(y,\mathbf{v})$ over angles, ν_{ea} is the electron-atom collision frequency. Since f_e also contains electrons reflected from the wall, it depends in general on η.

For ion distribution function $\mathrm{f}_i(y,\mathbf{v})$ we also consider collisions with neutral background only. In many discharges collisions of charged particles with neutrals dominate due to typically larger density of the neutral particles and larger cross-sections for that type of collisions. Therefore, for ions we have

$$v\frac{\partial}{\partial y}\mathrm{f}_i + \frac{eE}{m_i}\frac{\partial}{\partial v}\mathrm{f}_i = \nu_{ia}(\mathrm{f}_{i,eq} - \mathrm{f}_i), \tag{5.2}$$

where $\mathrm{f}_{i,eq}(y,\mathbf{v})$ is the equilibrium distribution function of ions.

Boundary conditions. We assume similarly as before that the source of plasma is located at the symmetry plane $y = 0$. Newly created ions and electrons have Maxwellian distribution functions of specified temperatures. We assume that the intensity of the source is given which means that the ion and electron currents (to the wall at $y = L$) are known, being equal in absolute values and having opposite signs, so the total current balance satisfies $j_i + j_e = 0$. The electrons and ions when crossing the source plane regain their original Maxwellian distributions. On the other hand, electrons reaching the wall undergo specular reflection with probability η or get absorbed with probability $1-\eta$. For simplicity we assume that η is independent of the energy of the incident electron. We also assume that ions are neutralized when they reach the wall.

For a given electric field, the equations for f_e and f_i can be solved using the characteristics. Characteristic lines for ion equation starting from $y = 0$ reach the wall, while the characteristics for the electron equation either reach the wall or return to the source, depending on the electron initial velocity. When the characteristics reach the wall they return but in this case the returned distribution function f_e is the incident distribution multiplied by η.

Statement. Now we notice that for the given electric field $E(y)$ ($E(y) \geq 0$) and the above stated boundary conditions the distribution functions f_e and f_i

can be determined from Eq. (5.1) and Eq. (5.2). This means that the charge densities n_i, n_e can be also determined. On the other hand, the electric field potential satisfies the Poisson equation

$$\varepsilon_0 \frac{\mathrm{d}^2\varphi}{\mathrm{d}y^2} = -e(n_i - n_e) \tag{5.3}$$

and the boundary conditions, or rather the initial conditions are $\varphi_0 = 0$, $E_L = -\frac{\mathrm{d}\varphi}{\mathrm{d}y}|_{y=L} = 0$, resulting from the fact that $y = 0$ is the symmetry plane of the problem. Consequently, the electric field at $x = L$ is already determined (for a given η). The perfect absorber case $\eta = 0$ would imply that the electric field E_L and thus the surface electric charge density at the wall is uniquely determined, regardless of the physical properties of the wall. This short reasoning shows that taking collisions into account does not change the main conclusion of this work. Following this simplified scheme of reasoning one can easily take into account other possible processes such as Coulomb collisions.

6. Conclusions

We expect that the problem of the Debye sheath formation between the plasma and the floating wall should have unique solution, provided that the following conditions are given: a) the efficiency of the plasma source; b) the distance L between the source and the wall; c) the electric field at the wall. Of course, the source efficiency must also contain information about the distribution functions of the created particles (electrons and ions), while c) tells us about the source properties – how many electrons can the wall absorb without returning them back to the plasma. It is clear that we talk about a dynamic quantity here. For a given flux of bombarding electrons some equilibrium should be established, so the wall's capacitance (the ability to hold a charge) likely depends on the intensity of the bombarding flux. However, by changing, for example, the wall temperature or the material from which it is made, we can influence this capacitance and thus the electric field at the wall surface.

Using the collisionless model, we began our considerations with a rather fictitious wall, which can be considered a physical idealization, i.e., a wall that does not absorb electrons at all. If the wall contains no trapped electrons, the electric field at its surface vanishes, $E_L = 0$. Therefore, all electrons are either reflected or neutralized by ions at the wall surface.

We can imagine an equilibrium situation in which all incoming to the wall electrons are neutralized by ions. For this to happen, a potential drop must be established so that the number of electrons reaching the wall is equal to the number of arriving ions. Clearly, at the beginning, when the sheath is not yet formed, the flux of electrons is much greater, so most of electrons must be reflected. Thus, the wall would act as a perfect absorber when the equilibrium

(stationary state) is achieved. We would then have a case of a "perfect absorber in the weak sense". However, it turns out that such a solution does not exist. Indeed, for equal fluxes of incident electrons and ions, (characterized in the model by $\eta = 0$) the zero electric field solution at the wall gives complex-valued electric field within a certain region of the domain $(0, L)$. For a solution to exist for given $L > 0$ and given source properties, we must assume that a certain, well defined, number of electrons must be reflected, so there is exactly one "effective reflection coefficient" η, $0 < \eta < 1$, for which there is a solution representing the sheath. In most cases, when speaking about a perfect absorber, authors mean what we call here "perfect absorber in the weak sense", although in numerical simulations this assumption is used also in the process of sheath formation.

It should be noted here that the assumption that the wall acts as a weak absorber does not concern the properties of the wall, but rather the value of the potential drop. Then, it is assumed that the electric field is formed in such a way that it deflects most of the electrons, and exactly as many ions as reach the wall. The opposite is true for a perfect absorber, where the wall always absorbs excess electrons.

A similar situation occurs in general case. Suppose L and the source efficiency are given. For a solution representing the Debye sheath with the predetermined electric field E_L at the wall to exist, we must assume that a certain fraction (defined by η) of the incident electrons is reflected from the wall. As we have already discussed, E_L determines the wall's ability to retain absorbed electrons.

As we argue in the previous section, taking collisions into account should not have a significant impact on the mathematical formulation of the problem and the general properties of the solution. To have a unique sheath solution for the given size L and the specified source additional assumptions are needed, such as the perfect absorber assumption, which in our opinion, is too restrictive. For example, in [13] where the plasma source-wall model that we use is also employed, the perfect absorber assumption is applied without specifying the domain size L. Instead, it is assumed that at the inflection point of the electric potential profile $\varphi(y)$ the electric field takes on a zero value. Numerical simulations show that indeed, for a large value of L, the electric potential profile exhibits strong drops near the source and the wall, separated by a plateau region with the inflection point somewhere in the middle. This suggest that at the inflection point, where the electric field reaches a minimum ($n_i = n_e$), the field is very close to zero.

The first strong potential drop near the source plays a role of a presheath where ions are accelerated to velocities close to the Bohm velocity, while the second one near the wall models the Debye sheath. For a large L, the lack of collisions results in the appearance of a broad plateau between these layers. If collisions were taken into account, the presheath would extend into the plateau region.

As was shown in our calculations, the vanishing of the electric field at the inflection point implies that L becomes infinite, although the obtained potential drop seems to be realistic (very close to the values that correspond to the finite but sufficiently large L). For finite positive values of the field at the inflection point, one obtains finite values of L. Hence, by assuming an electric field at the inflection point we determine the domain size and consequently the electric field E_L at the wall surface. It is observed that the potential drop also depends on L.

The vanishing electric field condition is often used as an assumption defining the edge of a Debye sheath in a multiscale analysis. However, GODYAK and STENBERG [31] note that this assumption also leads to the infinite separation of the sheath edge from the wall.

The dependence of the plasma potential on the spatial size of the problem can be also found in models that assume electrons in thermal equilibrium whereas ions are treated kinetically. For example, the pioneering work by TONKS and LANGMUIR [32] or [33, 34]. These models assume plasma generation in the entire domain and define the ionization source to be either constant or proportional to the electron density $n_0 \exp\left(-\frac{e\varphi}{kT_e}\right)$. This means that for different size of the region the ion current density towards the wall is different, making it difficult to compare to the presented model in which plasma generation is a fixed value. Nevertheless, the different nature of the dependence in those models, compared to the one shown in the present paper, is evident from the aforementioned difference in the assumptions.

For a sufficiently large L we observe the existence of a plateau of the electric potential profile with the inflection point in the middle. The plateau is observed for different η. In this case, for a given $1 > \eta > 0$ we can solve a slightly easier problem by assuming the vanishing electric field at the inflection point (as it is done in [13, 14]) and still obtain a good approximation of the potential drop.

Of course, the considered in this work model is based on many simplifications such as lack of collisions, localization of plasma source at $y = 0$ plane, electron backscattering that is independent on the incident electron energy and the absence of secondary electrons. It is certainly possible to model more intricate scenarios using numerical models, such as 2d collisional sheath with non-uniform magnetic field [35], or to kinetically model collisional effects (and even time dependence) in the two scale analysis [36, 37], or to include lateral energy components and more complex electron-wall interactions to the collisionless source-wall model [38, 39]. We, however, opted for a simplified model as the main goal is to demonstrate that the often-made assumption that the wall acts as an ideal absorber is physically incorrect not only in the sheath formation process but also at the equilibrium state. Furthermore, if we are interested in the time of sheath formation, this assumption can lead to large errors.

Finally, let us note that the case when the plasma is produced in the entire volume can be also treated similarly as we did in Section 5, so this too, we believe, will not change the main conclusion that the assumption of a perfect absorber leads to an overdetermined problem.

References

1. K.U. Riemann, *Kinetic theory of the plasma sheath transition in a weakly ionized plasma*, The Physics of Fluids, **24**, 12, 2163–2172, 1981, https://doi.org/10.1063/1.863332.
2. J.T. Scheuer, G.A. Emmert, *A collisional model of the plasma presheath*, The Physics of Fluids, **31**, 6, 1748–1756, 1988, https://doi.org/10.1063/1.866663.
3. K.U. Riemann, *The Bohm criterion and boundary conditions for a multicomponent system*, IEEE Transactions on Plasma Science, **23**, 4, 709–716, 1995, https://doi.org/10.1109/27.467993.
4. K.U. Riemann, *Plasma-sheath transition in the kinetic Tonks-Langmuir model*, Physics of Plasmas, **13**, 6, 063508, 2006, https://doi.org/10.1063/1.2209928.
5. F.X. Bronold, R.L. Heinisch, J. Marbach, H. Fehske, *Plasma walls beyond the perfect absorber approximation for electrons*, IEEE Transactions on Plasma Science, **39**, 2, 644–651, 2011, https://doi.org/10.1109/TPS.2010.2094209.
6. H.S.W. Massey, E.H.S. Burhop, *Electronic and Ionic Impact Phenomena*, Clarendon Press, Oxford, 1952.
7. H.D. Hagstrum, *Low energy de-excitation and neutralization processes near surfaces*, Inelastic Ion-Surface Collisions, N.H. Tolk, J.C. Tully, W. Heiland, C.W. White [eds.], pp. 1–25, Elsevier, 1977, https://doi.org/10.1016/b978-0-12-703550-5.50006-6.
8. H. Kersten, H. Deutsch, M. Otte, G. Swinkels, G. Kroesen, *Micro-disperse particles as probes for plasma surface interaction*, Thin Solid Films, **377-378**, 530–536, 2000, https://doi.org/10.1016/S0040-6090(00)01439-5.
9. M.Y. Ye, S. Takamura, *Effect of space-charge limited emission on measurements of plasma potential using emissive probes*, Physics of Plasmas, **7**, 8, 3457–3463, 2000, https://doi.org/10.1063/1.874210.
10. A. Dove, M. Horanyi, X. Wang, M. Piquette, A.R. Poppe, S. Robertson, *Experimental study of a photoelectron sheath*, Physics of Plasmas, **19**, 4, 043502, 2012, https://doi.org/10.1063/1.370170.
11. A. Palov, H. Fujii, S. Hiro, *Monte Carlo simulation of 1 eV–35 keV electron scattering in teflon*, Japanese Journal of Applied Physics, **37**, 11R, 6170, 1998, https://doi.org/10.1143/JJAP.37.6170.
12. J. Vaughan, *A new formula for secondary emission yield*, IEEE Transactions on Electron Devices, **36**, 9, 1963–1967 1989, https://doi.org/10.1109/16.34278.
13. L.A. Schwager, C.K. Birdsall, *Collector and source sheaths of a finite ion temperature plasma*, Physics of Fluids B: Plasma Physics, **2**, 5, 1057–1068, 1990, https://doi.org/10.1063/1.859279.

14. L.A. SCHWAGER, *Effects of secondary and thermionic electron emission on the collector and source sheaths of a finite ion temperature plasma using kinetic theory and numerical simulation*, Physics of Fluids B: Plasma Physics, **5**, 2, 631–645, 1993, https://doi.org/10.1063/1.860495.

15. R.J. PROCASSINI, C.K. BIRDSALL, E.C. MORSE, *A fully kinetic, self-consistent particle simulation model of the collisionless plasma–sheath region*, Physics of Fluids B: Plasma Physics, **2**, 12, 3191–3205 1990, https://doi.org/10.1063/1.859229.

16. T. GYERGYEK, J. KOVAČIČ, *Saturation of a floating potential of an electron emitting electrode with increased electron emission: A one-dimensional kinetic model and particle-in-cell simulation*, Physics of Plasmas, **19**, 1, 013506, 2012, https://doi.org/10.1063/1.3677359.

17. A. DENIG, K. HARA, *Kinetic Model of Plasma Sheath Near a Dielectric-Coated, Metal Wall*, 37th International Electric Propulsion Conference, IEPC-2022-345, 2022.

18. K.U. RIEMANN, *Theory of the plasma-sheath transition*, Journal of Technical Physics, **41**, 1, 89–121, 2000.

19. D. BOHM, *Minimum ionic kinetic energy for a stable sheath*, The Characteristics of Electrical Discharges in Magnetic Fields, A. Guthrie, R.K. Wakerling [eds.], pp. 77–86, McGraw Hill, New York, NY, 1949.

20. S. KUHN, *Axial equilibria, disruptive effects, and Buneman instability in collisionless single-ended Q-machines*, Plasma Physics, **23**, 10, 881, 1981, https://doi.org/10.1088/0032-1028/23/10/002.

21. N. STERNBERG, V. GODYAK, *The Bohm plasma-sheath model and the Bohm criterion revisited*, IEEE Transactions on Plasma Science, **35**, 5, 1341–1349, 2007, https://doi.org/10.1109/TPS.2007.905944.

22. G.D. HOBBS, J.A. WESSON, *Heat flow through a Langmuir sheath in the presence of electron emission*, Plasma Physics, **9**, 1, 85, 1967, https://doi.org/10.1088/0032-1028/9/1/410.

23. V.I. DEMIDOV, S.V. RATYNSKAIA, K. RYPDAL, *Electric probes for plasmas: The link between theory and instrument*, Review of Scientific Instruments, **73**, 10, 3409–3439, 2002, https://doi.org/10.1063/1.1505099.

24. D.W. VANCE, *Surface charging of insulators by ion irradiation*, Journal of Applied Physics, **42**, 13, 5430–5443 1971, https://doi.org/10.1063/1.1659961.

25. H. WINTER, *Scattering of atoms and ions from insulator surfaces*, Progress in Surface Science, **63**, 7, 177–247, 2000, https://doi.org/10.1016/S0079-6816(99)00020-9.

26. N. TANAKA, F. IKEMOTO, I. YAMADA, Y. SHIMABUKURO, M. KISAKI, W.A. DIÑO, M. SASAO, M. WADA, H. YAMAOKA, *Positive and negative hydrogen ion reflections of low-energy atomic and molecular hydrogen ion beam from HOPG and Mo surfaces*, Review of Scientific Instruments, **91**, 1, 013313, 2020, https://doi.org/10.1063/1.5129576.

27. R. BEHRISCH, W. ECKSTEIN, *Ion backscattering from solid surfaces*, Physics of Plasma-Wall Interactions in Controlled Fusion, D.E. Post, R. Behrisch [eds.], pp. 413–438, Springer, US, Boston, MA, 1986, https://doi.org/10.1007/978-1-4757-0067-1_10.

28. P.J. MARTIN, *Ion-based methods for optical thin film deposition*, Journal of Materials Science, **21**, 1, 1–25, 1986, https://doi.org/10.1007/bf01144693.

29. J. Cuthbertson, W. Langer, R. Motley, *Reflection of low energy plasma ions from metal surfaces*, Journal of Nuclear Materials, **196-198**, 113–128, 1992, https://doi.org/10.1016/S0022-3115(06)80017-6.

30. H.D. Hagstrum, *Reflection of noble gas ions at solid surfaces*, Physical Review, **123**, 758–765, 1961, https://doi.org/10.1103/PhysRev.123.758.

31. V. Godyak, N. Sternberg, *On the consistency of the collisionless sheath model*, Physics of Plasmas, **9**, 11, 4427–4430, 2002, https://doi.org/10.1063/1.1513155.

32. L. Tonks, I. Langmuir, *A general theory of the plasma of an arc*, Physical Review, **34**, 876–922, 1929, https://doi.org/10.1103/PhysRev.34.876.

33. S.A. Self, *Exact solution of the collisionless plasma-sheath equation*, The Physics of Fluids, **6**, 12, 1762–1768, 1963, https://doi.org/10.1063/1.1711020.

34. G.A. Emmert, R.M. Wieland, A.T. Mense, J.N. Davidson, *Electric sheath and presheath in a collisionless, finite ion temperature plasma*, The Physics of Fluids, **23**, 4, 803–812, 1980, https://doi.org/10.1063/1.863062.

35. A. Lopez Ortega, I.G. Mikellides, *2D fluid-PIC simulations of hall thrusters with self-consistent resolution of the space-charge regions*, Plasma, **6**, 3, 550–562, 2023, https://doi.org/10.3390/plasma6030038.

36. D.D. Tskhakaya, I. Vasileska, L. Kos, N. Jelić, S. Kuhn, *Time-dependent kinetic theory of the plasma-wall transition layer in a weakly ionized plasma*, Physics of Plasmas, **27**, 2, 023517, 2020, https://doi.org/10.1063/1.5123911.

37. D.D. Tskhakaya, I. Vasileska, L. Kos, *Time-dependent behavior of a Debye sheath: Lengthening and establishment of the stationary state*, Physics of Plasmas, **28**, 6, 063511, 2021, https://doi.org/10.1063/5.0046308.

38. K. Rasek, F.X. Bronold, H. Fehske, *Kinetic modeling of the electric double layer at a dielectric plasma-solid interface*, Physical Review E, **102**, 023206, 2020, https://doi.org/10.1103/PhysRevE.102.023206.

39. K. Rasek, F.X. Bronold, H. Fehske, *Charge kinetics across a negatively biased semiconducting plasma-solid interface*, Physical Review E, **105**, 045202, 2022, https://doi.org/10.1103/PhysRevE.105.045202.

Received April 29, 2025; revised version August 15, 2025.
Published online October 2, 2025.